HHS Public Access

Author manuscript

Cells Tissues Organs. Author manuscript; available in PMC 2018 May 29.

Published in final edited form as:

Cells Tissues Organs. 2017 ; 203(3): 183–193. doi:10.1159/000455070.

Characterization of an Acellular Scaffold for a Tissue Engineering Approach to Nipple—Areolar Complex Reconstruction

Nicholas C. Pashos, BS[1,2], **Michelle E. Scarritt, Ph.D.**[1], **Zachary R. Eagle**[1], **Jeffery M. Gimble, M.D., Ph.D.**[1,4], **Abigail Chaffin, M.D.**[3], and **Bruce A. Bunnell, Ph.D.**[1,5]

[1]Center for Stem Cell Research and Regenerative Medicine, Tulane University School of Medicine, New Orleans, LA 70112

[2]Bioinnovation PhD Program, Tulane University, School of Science and Engineering, New Orleans LA 70118

[3]Department of Surgery, Tulane University School of Medicine, New Orleans, LA 70112

[4]LaCell LLC, New Orleans, LA 70112

[5]Department of Pharmacology Tulane University School of Medicine, New Orleans, LA 70112

Abstract

A significant number of patients undergo mastectomies and breast reconstructions every year using many surgical-based techniques to reconstruct the nipple-areolar complex (NAC). Described herein is a tissue engineering approach that may permit a human NAC onlay graft during breast reconstruction procedures. By applying decellularization, the removal of cellular components from tissue, to an intact whole donor NAC, the extracellular matrix (ECM) structure of the NAC is preserved; thereby, creating a biologically derived scaffold for cells to repopulate and regenerate the NAC. A detergent-based decellularization method was used to derive whole-NAC scaffolds from non-human primate *rhesus macaque* NAC tissue. Using both histological and quantitative analyses for the native and decellularized tissues, the derived ECM graft was assessed. Bioactivity of the scaffold was evaluated following cell culture with bone-marrow-derived stem cells (BMSC). The data presented here demonstrate that scaffolds are devoid of cells and retain ECM integrity and a high-degree of bioactivity. The content of collagen and glycosaminoglycans (GAGs) were not significantly altered by the decellularization process; where as, elastin content was significantly decreased. The proliferation and apoptosis of seeded BMSCs were found to be ~65%

*Corresponding Author: Bruce A. Bunnell, PhD, Professor and Director, Center for Stem Cell Research and Regenerative Medicine, Department of Pharmacology, Tulane University School of Medicine, 1430 Tulane Avenue, SL-99, New Orleans, LA 70112, Phone: (504) 988-7711, Fax: (504) 988-7710, bbunnell@tulane.edu.

[1]A portion of this paper was presented as a poster at the American Society of Gene and Cell Therapy Conference; 2015; New Orleans, LA

Disclosure: The first and corresponding authors do not have any disclosures. J. Gimble, is the co-founder, co-owner and Chief Scientific Officer of LaCell LLC.

Author Contributions: N.P. M.S., BAB, J.G and A.C. helped in initial design and write and/or editing of manuscript. N.P., M.S. and Z.E. carried out experimentation

Disclosure: B. Bunnell and N. Pashos are the listed inventors of a patent application filing, with assignee of Tulane University, based off of the data presented in this manuscript. J. Gimble, is the co-founder, co-owner and Chief Scientific Officer of LaCell LLC.

and <1.5%, respectively. This study characterizes the successful decellularization of NAC tissue as compared to native NACs based on structural protein composition, lubricating protein retention, maintenance of adhesion molecules, and bioactivity when reseeded with cells. These histological and quantitative analyses provide the foundation for a novel approach to NAC reconstruction.

Keywords

Nipple-areolar complex reconstruction; tissue engineering; regenerative medicine; acellular; matrix

1. Introduction

Current strategies for nipple-areolar complex (NAC) reconstruction in breast cancer patients are limited to surgical techniques that create a NAC structure from existing local tissue, secondary site grafting, 3D tattooing (Halvorson, Cormican et al. 2014, Jordan, Khavanin et al. 2014), or using commercial acellular dermal matrix sheets (Craft and May 2011, Seaman, Akbari et al. 2012). These surgical strategies, although offering breast reconstruction patients a NAC-like structure, are highly variable. Generating a biocompatible NAC graft from decellularized human intact NAC is a promising alternative approach to reconstruction following mastectomies. Herein, a tissue engineered, regenerative medicine approach to reconstruct the NAC using a biologically derived scaffolds and autologous cell sources is described.

There are more than 2.8 million breast cancer survivors in the United States and 230,000 newly diagnosed cases per year (2014, Howlader N 2014). Approximately 36% of patients with early stage diagnoses and 60% of patients with late stage diagnoses undergo mastectomies (Siegel, DeSantis et al. 2012). Moreover, immediate breast reconstruction following mastectomy has become more common, increasing from 20.8% in 1998 to 37.8% in 2008 (Albornoz, Bach et al. 2013). This is not surprising, as breast reconstruction is known to provide psychological benefits for women who undergo mastectomies. There is evidence to suggest that NAC reconstruction affects psychological well-being by enhancing body image and self-esteem or by decreasing the feeling of distress due to the mastectomy procedure itself (Al-Ghazal, Fallowfield et al. 2000, Nano, Gill et al. 2005, Lohsiriwat and Petit 2012). Evidence also suggests that women are more comfortable with getting a mastectomy if the nipple can be spared or reconstructed (Didier, Arnaboldi et al. 2012). To date, no tissue engineering strategies have been developed that focus on reconstruction of the NAC. The application of decellularization to the whole, semi-glandular NAC has the potential to create a non-immunogenic scaffold that retains the microarchitecture and gross structures of a native NAC. This tissue engineering approach to whole structure regeneration allows for the effective removal of cellular material, the preservation of the extracellular matrix composition and structure, and retention of cell adhesion molecules (Scarritt, Pashos et al. 2015). Once decellularized, NAC scaffolds can be seeded with autologous cells to create an onlay graft that is patient-specific (Figure 1). In addition, this technique generates a whole NAC graft that aesthetically and molecularly mimics the native nipple.

Materials and Methods

Decellularization

Veterinary technicians at Tulane National Primate Research Center (TNPRC) collected rhesus macaque (*Macaca mulatta*) NAC tissue from disease-free animals undergoing routine euthanasia due to chronic diarrhea or self-mutilation as well as control animals from various experiments. All animal procedures conformed to the requirements of the Animal Welfare Act and all animal protocols were approved by the Institutional Animal Care and Use Committee (IACUC) of the TNPRC before implementation of experimental protocols. NAC from females and males ranging from 1-13 years of age were used.

Rhesus macaque tissue samples were decellularized through a modified protocol previously described by Bonvillain *et al.* (2012) and Scarritt *et al.* (2014). In brief, after NAC samples were collected, they were incubated with the Triton X100 detergent solution followed by 2 hours in water. Next, NACs were incubated with the sodium deoxycholate solution (Fisher Scientific, Fairlawn NJ, USA, cat: BP349,)followed by 2 hours in water. The samples were incubated in sodium chloride for 2 hours, followed by a 2 hour water wash. Samples were then incubated overnight at 4°C in a PBS solution containing 5× antibiotic/antimycotic. After overnight incubation, samples were water washed for 2 hours, treated with DNase I (Sigma, St. Louis, MO, USA, cat: DN25) for 2 hours, washed with water for 2 hours, and then stored in a PBS solution containing 5× antibiotic/antimycotic at 4°C until use.

Genomic DNA and fragment analysis

Samples were frozen at -80°C and then lyophilized for 48 hours using a ModulyoD FreezeDryer (Thermo Electron Corporation) set to -40°C and 80 mmHg. Using sterile tools, three random portions of the lyophilized samples were dissected, shredded with forceps, and weighed. The samples were processed in triplicate using a Qiagen DNeasy kit (Valencia, CA) according to the manufacturer's instructions. The concentration of genomic DNA (gDNA) was quantified using a NanoDrop spectrophotometer (Thermo-Fisher Scientific, Waltham, MA). The gDNA recovered from all samples was precipitated by addition of sodium acetate (final concentration of 0.3M) and 0.7 volumes of 2-propanol. Samples were centrifuged at 15,000 × g at 4°C for 22 minutes. The resulting pellet was washed with 70% ethanol, centrifuged again for 10 minutes, decanted, and air dried for 15 minutes. The pellet was resuspended to 1.0 ug/uL in DNA elution buffer (Qiagen DNeasy kit). gDNA fragment sizes were evaluated by gel electrophoresis through a 1.0% Ultrapure agarose gel (Invitrogen) with 0.07% ethidium bromide (Promega Corporation, Madison, WI). Lastly, 1.5 μg of DNA from each sample was loaded and electrophoresed at 100 volts for 1 hour and 15 minutes. An ImageQuant LAS 4000 (GE) was used to image the gels.

Histological analysis

Tissue embedding, sectioning, and staining were completed through the Histology Core at the Center for Stem Cell and Regenerative Medicine at Tulane University School of Medicine. Hematoxylin and eosin (H&E) staining for nuclei and matrix protein structures, Gomori Trichrome staining for collagen, and Movat's Modified Pentachrome staining for

elastin were accomplished using standard procedures. All histological analyses had sample sizes of three for each group.

Alcian Blue staining for glycosaminoglycans (GAGs) was completed with (GX8, Acros Organics, NJ, USA cat: 400460250) and countered stained with Safranin O staining. The protocol used was a modified version of the established Abcam protocol (ab150662 Alcian Blue Mucin Stain).

Immunohistochemical (IHC) analyses of extracellular matrix (ECM) adhesion molecules employed primary murine monoclonal antibodies for laminin (Chemicon, cat: 88918) and fibronectin (Iowa Hybridoma, P1h11). A horseradish peroxidase conjugated goat anti-mouse secondary antibody (Santa Cruz Biotechnology, Dallas, TX USA, cat: SC-2005) was used with all adhesion molecule IHC evaluations. Primary antibodies were used at a dilution of 1:200 and secondary antibody was used at dilution of 1:400. An IgG1 control (R&D System, cat: MAB398) was used to confirm antibody specificity. After deparaffinization and rehydration through ethanol, tissue sections were boiled for 10 minutes in sodium citrate buffer. Sections were blocked for 30 minutes with PerkinElmer Blocking Reagent (PerkinElmer, cat: FP1136), washed 3× with Tris-buffered saline (TBS; 50 mM Tris, 150 mM NaCl, pH 7.6), and then incubated overnight at 4°C with the primary antibody or IgG1 control in a humidified chamber. The following day, samples were washed with TBS and incubated with secondary antibody at room temperature for 1 hour in a humidified chamber. After washing with TBS, sections were counter-stained with Mayer Modified Hemotoxylin (Newcomer Solutions, Madison, WI cat 1202). IHC was imaged using an Aperio ScanScope (Aperio, Vista, CA) at a magnification of 40×. Images were analyzed using the Aperio ImageScope program.

DAPI staining of tissue sections was conducted for visualization of intact nuclei. Tissue sections were prepared as previously described. DAPI (Invitrogen) staining was imaged using a Leica DMRXA2 deconvolution inverted fluorescent microscope (Leica Microsystems, Buffalo Grove, IL) fitted with the Cooke SensiCAM camera/controller and Slidebook software.

Total protein and GAG quantification

Samples were frozen at -80°C and lyophilized. Using sterile tools, three random portions of the lyophilized samples were dissected, minced with forceps, and massed to approximately 100 mg per sample. The samples were then digested and processed as previously detailed (Bonvillain, Scarritt et al. 2013, Scarritt, Bonvillain et al. 2014).

Collagen quantification

Using the Total Collagen kit (QuickZyme Biosciences, Leiden, Netherlands), collagen was quantified according to the manufacturer's instructions. In brief, 10mg of lyophilized tissue were used for each triplicate native and acellular test group. The samples underwent hydrolysis in 6M HCl overnight at 95°C, followed by oxidation of hydroxyproline. Stained hydroxyproline from samples and standards were read on a FLUOstar Optima microplate reader at 545nm.

Elastin quantification

Elastin was quantified using the Fastin Elastin Assay Kit and protocol (Biocolor Life Science Assays, Carrickfergus, United Kingdom). In brief, lyophilized samples were treated with 0.25 M oxalic acid and incubated at 100°C, to solubilize the elastin. Elastin was extracted from three incubations in oxalic acid. Extracts elastin was precipitated, concentrated, and stained. Absorbance was read at 513nm using a BioRad SmartSpec Plus spectrophotometer.

Dynamic cell seeding

Bone marrow-derived mesenchymal stem cells (BMSCs) from rhesus macaques (*Macca mulatta*) were isolated and characterized by the TNPRC Division of Regenerative Medicine Core. Passage 3 cells BMSCs were plated at 150 cells per cm^2 onto a 15 cm^2 tissue-culture treated dish. Acellular scaffolds were pre-conditioned with cell growth media in a cell culture incubator at 5% CO_2 and 95% O_2 for approximately 30 minutes prior to seeding. Three to five pre-conditioned acellular scaffolds of dimensions 7mm × 7mm × 2mm were then placed into a non-treated sterile 10 cm^2 plate. Scaffolds were submerged in complete conditioned media (α-modified Eagle's medium containing 16.4% fetal bovine serum, 4 mM L-glutamine, 100 U/mL penicillin, 100 ug/mL streptomycin, and 250 ng/mL amphotericin B). Samples were placed on an orbital rotating shaker in a tissue culture incubator and agitated at a continuous low speed; and approximately 1×10^6 BMSCs were then added per sample.

Seeded scaffolds were removed for analysis at 1, 2, and 7 days for cell proliferation [Proliferating cellular nuclear antigen (PCNA), Abcam ab29)] and apoptosis [TdT-mediated dUTP Nick-end Labeling (TUNEL)]. TUNEL protocol was performed as previously described (Bonvillain, Danchuk et al. 2012). For assessing cell proliferation, tissue sections were blocked for 15 minutes with 5% BSA, incubated with primary antibody at a dilution of 1:6 000, washed with TBS, and then incubated with secondary antibody at a concentration of 1:200 (Santa Cruz: Alexaflour 488, goat anti mouse). Cell proliferation (n=4) and apoptosis (n=4) were imaged using a Leica DMRXA2 deconvolution inverted fluorescent microscope (Leica Microsystems, Buffalo Grove, IL) fitted with the Cooke SensiCAM camera/controller and Slidebook software. 10 images at 10× were taken of each biological replicate and blind counted.

Live/ dead assay of the NAC scaffold was performed in 6-well plates with a cellular density of ~3.5×10^5 per well, with one 5 mm dimeter and 2-3mm depth scaffold in each well. NACs scaffold were taken from 3 donor NHP (n=4), a no scaffold control (n=4) and a commercially available porcine dermal scaffold, Strattice, (n=4). Using trypan blue exclusion cell viability was evaluated at 12 hours, 24 hours and 48 hours after cell adhesion. All media was collected, wells were trypsinized for 3 minutes, neutralized with equal volume of cell culture media and combined with previously collected media. Cells were stained using trypan blue (0.4%, Gibco 15250) and counted on a hemocytometer. Cell viability ([1-(dead cell count /total cell count)] *100%) was calculated per well and averaged for each group.

Statistics

Statistical significance was determined by two-tailed t-tests or two-way ANOVA. For all analyses, an n=3 or greater number of experiments were conducted. A p-value ≤ 0.05 was considered significant and is designated by an asterisk (*). Numerical values are presented as average ± SEM. All calculations and graphs were completed in GraphPad Prism, Version 5.03.

Results

Nuclei are removed by decellularization

H&E staining of native NAC tissue showed dense eosin staining in the keratinocyte layer of the epidermis (Figure 2). Blood vessels structures, surrounded by darkly stained cell nuclei in the native samples, are still visible in the decellularized NAC (yellow arrows, Figure 2). Decellularized macaque NAC tissue showed a lack of hematoxylin-stained nuclei indicating efficient cell removal (Figure 2). Complete cell removal was also observed within areas of dense collagen (Figure 2). DAPI staining of decellularized tissue sections revealed that there were no intact nuclei in NAC scaffolds as compared to the native NAC, which showed heavy nuclear staining throughout the tissue (Figure 2).

Genomic DNA isolation, quantification, and fragment analysis reveals decellularization reduces DNA content

Native NAC contained 1905±422.1 ng DNA per mg lyophilized tissue, while decellularized NAC contained significantly less DNA at 56.51±8.45 ng/mg. Gel electrophoresis of 1 μg of pooled gDNA from native NAC appeared as a dark, dense, high molecular weight band; whereas, pooled DNA isolated from decellularized NAC did not create any visible banding, consistent with degradation and/or removal (Figure 3).

Extracellular matrix structure and composition following decellularization

NAC tissue sections were stained with Gomori Trichrome for collagen, Movat's Modified Pentachrome for elastin, and Alcian Blue for glycosaminoglycans (GAGs). Collagen fibers (green) were well-preserved throughout decellularized NAC in a pattern comparable to native NAC (Figure 2). Similarly, elastin and GAGs were also visible in decellularized NAC; however, the staining for elastin and GAGs was less intense in decellularized NAC in comparison to native NAC. This decrease may be attributed, in part, to the removal of cellular content. To evaluate whether decellularization removes or damages collagen, elastin, or GAGs, colorimetric quantification assays were executed.

Native and decellularized NAC contained 46.12±13.88 and 128.57±55.05 μg collagen/mg dry tissue, respectively; indicating that collagen content was enriched for collagen but not significantly (Figures 2 & 3). Soluble tropoelastins, lathyrogenic elastin, α-elastin, and κ–elastin in native and decellularized NAC was quantified using a colorimetric assay. Decellularization significantly reduced elastin content from 25.03±0.93 to 7.77±2.84 μg/ mg of dry tissue (Figure 3). GAGs in native and decellularized NAC tissues were quantified using a colorimetric assay. GAG content was measured as a ratio to total protein concentrations and was determined to be 0.037±0.009 for the native tissue and 0.065±0.027

for the decellularized tissue (Figure 3). There was no significant decrease in GAG content after decellularization.

To determine the presence and localization of the cell adhesion molecules fibronectin and laminin, immunohistochemistry was used for visual analysis. Laminin was found to be present throughout the matrix of both the native and decellularized NAC with concentrated staining in the epidermis where a dense layer of keratinocytes resides (Figure 4). Fibronectin was seen ubiquitously throughout the acellular and native samples as well, but was most concentrated in the dermis layers (Figure 4). Both secondary antibody only and serotype (IgG1) controls confirmed that there was minimal background staining and non-specific staining present (Figure 4).

Dynamic cell seeding of stem cells demonstrates bioactivity of decellularized NAC

H&E staining of re-seeded NAC tissue sections showed that cells initially attached to the periphery of the scaffold at days 1 and 2. As culture progressed, cells migrated deeper into areas of the NAC scaffold by day 7 (Figure 5). Seeded cells were evaluated for both cell proliferation and apoptosis after 1, 2, and 7 days of dynamic culture on NAC scaffolds. Less than 1% of the cells underwent apoptosis during the culture period. The percentage of cells undergoing proliferation was found to be 64.98±7.42 %, 62.38±2.34%, and 67.42±4.23% for day 1, 2 and 7, respectively (Figure 5). Additionally, cell viability was found to be greater than 90% for 12, 24 and 48-hour time points for all groups, no scaffold control: 93.18±1.39% (12hrs), 95.98±1.45% (24hrs), 94.39±0.69% (48hrs); commercially available acellular dermis control: 95.18±0.79% (12hrs), 95.97±1.03% (24hrs), 90.39±1.18% (48hrs); decellularized NAC scaffold: 94.92±0.95% (12hrs), 94.59±0.65% (24hrs), 91.14±1.62% (48hrs) (Figure 5).

Discussion

The lack of tissue engineering approaches for breast reconstruction led us to explore the potential application of decellularization to the structural and physical aesthetic uniqueness of the NAC. To achieve the overall goal of applying a decellularized whole NAC during the reconstruction process, the efficacy of the decellularization process was evaluated with respect to the removal of intact cells and debris without damaging the ECM. We have previously shown that non-human primate and rat lung tissues can be efficiently decellularized using a combination of detergents, salts, and enzymes (Bonvillain, Danchuk et al. 2012, Bonvillain, Scarritt et al. 2013, Scarritt, Bonvillain et al. 2014); however, decellularization of NAC posed distinct challenges, namely, the lack of an accessible vasculature for distribution of decellularization solutions throughout the tissue. To address this challenge, incubation time, detergent concentration, and physical agitation were optimized to permit the efficient decellularization of NAC. Efficacy of NAC decellularization was evaluated based on three key criteria, as outlined by Crapo *et al.* (2011), namely: (1) no visible signs of cells or cell debris, (2) significant reduction of DNA, and (3) degradation of any remaining DNA to less than 200 bp (Crapo, Gilbert et al. 2011). These criteria are based on the principle that cellular debris, substantially high concentrations of DNA, or the presence of long DNA fragments in a decellularized tissue are

potentially immunogenic and, therefore, possibly detrimental to successful incorporation post-transplantation. Decellularized human dermal products have been used clinically for 30+ years with no substantial evidence of immune rejection by the host (Wainwright, Madden et al. 1996, Harirchian and Baredes 2013, Scarritt, Pashos et al. 2015). The lack of immunogenicity of acellular dermal matrices has permitted them to be used in an estimated 56% of prosthetic breast reconstructions (Ho, Nguyen et al. 2012, Janis, O'Neill et al. 2012).

Decellularized rhesus macaque NAC tissue sections stained with H&E and DAPI showed no intact NAC nuclei. A greater than 97% reduction in genomic DNA was observed as compared to the native control, which is a significant minimization of the DNA content to less 56ng DNA/mg of dried tissue weight. Currently there are commercially available acellular products, such as TissueMend™, Restore™, GraftJacket™ and AlloDerm™, which have reported DNA contents of 794.6 ± 97.8, 526.8 ± 125.6, 134.6 ± 44.0 and 273 ± 169 ng DNA/mg dry tissue weight, respectively. (Choe and Bell 2001, Derwin, Baker et al. 2006, Moore, Samsell et al. 2015). Our observed residual DNA content in the NAC acellular graft is well below the threshold that is currently offered commercially and accepted clinically.

By maintaining both the micro and macro structures of the native tissue, the decellularized whole matrix offers a major potential advantage to the reconstruction of the NAC by allowing for an engineered tissue that aesthetically mimics that of the patients' pre-operative anatomy. To achieve this goal, it is essential that the extracellular components, such as collagen, elastin, GAGs, and cell adhesion molecules, are minimally disturbed during the decellularization process. Histological analysis through H&E showed that the primary structures of the NAC are maintained on the microscopic scale; the extracellular matrix fibers were intact and no nuclei were found in the acellular NAC. Gomori Trichrome staining showed that collagen, a major ECM component for the skin, was preserved. This was confirmed by colorimetric quantification of collagen hydroxyproline. From Movat's pentachrome staining, elastin fibers were visible in the decellularized NAC; however, the overall staining intensity, in comparison to native NAC, indicated a reduction in elastin. Colorimetric quantification confirmed that decellularization reduced the soluble elastin content of the NAC. Although this reduction in elastin may affect the mechanical parameters of the NAC and will be evaluated in future studies, this was an expected outcome of the detergent-based decellularization process. Elastin has been shown in previous studies to be significantly decreased during decellularization in a variety of tissue types (Petersen, Calle et al. 2012, Reimer, Syedain et al. 2016). However, it has also been observed that the native environment *in vivo* can restore levels of elastin and other extracellular proteins, such as collagens, after scaffolds are reincorporated into the body (Ghazanfari, Driessen-Mol et al. 2015, Reimer, Syedain et al. 2016). Alcian Blue staining of decellularized NAC samples confirmed the presence of GAGs, which are an important ECM component for lubrication. A slight decrease in the Alcian Blue staining intensity suggested that some of GAG content may have been lost during the decellularization process. However, GAG quantification using a colorimetric assay showed no significant decrease. Since proteoglycans are localized in both cells and extracellular matrix leading to an expectation that the GAGs would have some decrease after decellularization (Ferdous and Grande-Allen 2007, Petersen, Calle et al. 2012). These trends with respect to the color intensity for Gomori, Movat's, GAGs and/or

the ratio of GAG to total protein concentration were similar to those observed in rhesus macaque lung, rat lung, and porcine dermis (Hoganson, O'Doherty et al. 2010, Bonvillain, Danchuk et al. 2012, Scarritt, Bonvillain et al. 2014). Overall, these histologic analyses confirmed that the resulting NAC acellular matrix maintained its structure, shape, and composition.

The presence of cellular adhesion molecules in the decellularized matrix provides a basis for cellular attachment to and cellular migration in the acellular scaffold, lending to its bioactivity. In accordance with Hoganson *et al* (2010) and Walter *et al*. (2012) who previously demonstrated preservation of fibronectin and laminin after decellularization of porcine dermis (Walter, Matsuda et al. 1998, Hoganson, O'Doherty et al. 2010), we observed that both laminin and fibronectin were preserved; however they were differentially localized. Laminin was observed predominantly in the epidermis while fibronectin was expressed ubiquitously throughout the dermis.

To determine the bioactivity of the acellular NAC, the scaffold was seeded with rhesus macaque BMSCs. Cells were able to survive and proliferate throughout the 7 day culture with low percentages of cell death. Similarly, cell viability was found to be greater than 90% and no significant difference was observed between the NAC scaffold, commercially available acellular dermis and the no scaffold control. The H&E stained tissue sections show BMSCs attached to the periphery of the scaffold during early time points with cells migrating deeper into areas of the acellular scaffold by day 2 and 7. This preliminary evaluation of cell seeding indicated that the decellularized scaffold provides an environment permissible for adhesion and continuous growth of the seeded cells.

Conclusions

Whole NAC reconstruction using a tissue engineered acellular graft may provide a structural and cosmetic recreation of a patient's own NAC, thereby surpassing the currently available standard of care. The current study serves as an initial *in vitro* report establishing the feasibility of NAC tissue engineering strategies. Herein, the characterization of the decellularized NAC scaffold with comparison to the native NAC structure is reported as well as analyses of the isolated NAC scaffold's cellular bioactivity. This preliminary study sets the stage for further biological and material characterization of the acellular NAC graft, as well as the optimization of the decellularization process in anticipation of future clinical translation. Future in vivo studies will focus on the rate of NAC engraftment and neovascularization, using skin wound healing models with commercially available dermal matrices as a standard of care control comparison.

Acknowledgments

Nicholas C. Pashos is supported by an NSF IGERT training grant in Bioinnovation, DGE-1144646

References

Cancer Facts and Figures. Atlanta, GA: American Cancer Society; 2014. Cancer Facts and Figures 2014.

Al-Ghazal SK, Fallowfield L, Blamey RW. Comparison of psychological aspects and patient satisfaction following breast conserving surgery, simple mastectomy and breast reconstruction. Eur J Cancer. 2000; 36(15):1938–1943. [PubMed: 11000574]

Albornoz CR, Bach PB, Mehrara BJ, Disa JJ, Pusic AL, McCarthy CM, Cordeiro PG, Matros E. A paradigm shift in U.S. Breast reconstruction: increasing implant rates. Plast Reconstr Surg. 2013; 131(1):15–23. [PubMed: 23271515]

Bonvillain RW, Danchuk S, Sullivan DE, Betancourt AM, Semon JA, Eagle ME, Mayeux JP, Gregory AN, Wang G, Townley IK, Borg ZD, Weiss DJ, Bunnell BA. A nonhuman primate model of lung regeneration: detergent-mediated decellularization and initial in vitro recellularization with mesenchymal stem cells. Tissue Eng Part A. 2012; 18(23-24):2437–2452. [PubMed: 22764775]

Bonvillain RW, Scarritt ME, Pashos NC, Mayeux JP, Meshberger CL, Betancourt AM, Sullivan DE, Bunnell BA. Nonhuman primate lung decellularization and recellularization using a specialized large-organ bioreactor. J Vis Exp. 2013; 82:e50825.

Choe JM, Bell T. Genetic material is present in cadaveric dermis and cadaveric fascia lata. J Urol. 2001; 166(1):122–124. [PubMed: 11435837]

Craft RO, May JW. Staged nipple reconstruction with vascularized SurgiMend acellular dermal matrix. Plast Reconstr Surg. 2011; 127(6):148e–149e.

Crapo PM, Gilbert TW, Badylak SF. An overview of tissue and whole organ decellularization processes. Biomaterials. 2011; 32(12):3233–3243. [PubMed: 21296410]

Derwin KA, Baker AR, Spragg RK, Leigh DR, Iannotti JP. Commercial extracellular matrix scaffolds for rotator cuff tendon repair. Biomechanical, biochemical, and cellular properties. J Bone Joint Surg Am. 2006; 88(12):2665–2672. [PubMed: 17142417]

Didier F, Arnaboldi P, Gandini S, Maldifassi A, Goldhirsch A, Radice D, Minotti I, Ballardini B, Luini A, Santillo B, Rietjens M, Petit JY. Why do women accept to undergo a nipple sparing mastectomy or to reconstruct the nipple areola complex when nipple sparing mastectomy is not possible? Breast Cancer Res Treat. 2012; 132(3):1177–1184. [PubMed: 22350788]

Ferdous Z, Grande-Allen KJ. Utility and control of proteoglycans in tissue engineering. Tissue Eng. 2007; 13(8):1893–1904. [PubMed: 17518731]

Ghazanfari S, Driessen-Mol A, Sanders B, Dijkman PE, Hoerstrup SP, Baaijens FP, Bouten CV. In Vivo Collagen Remodeling in the Vascular Wall of Decellularized Stented Tissue-Engineered Heart Valves. Tissue Eng Part A. 2015; 21(15-16):2206–2215. [PubMed: 26028124]

Halvorson EG, Cormican M, West ME, Myers V. Three-dimensional nipple-areola tattooing: a new technique with superior results. Plast Reconstr Surg. 2014; 133(5):1073–1075. [PubMed: 24776543]

Harirchian S, Baredes S. Use of AlloDerm in primary reconstruction after resection of squamous cell carcinoma of the lip and oral commissure. Am J Otolaryngol. 2013; 34(5):611–613. [PubMed: 23558359]

Ho G, Nguyen TJ, Shahabi A, Hwang BH, Chan LS, Wong AK. A systematic review and meta-analysis of complications associated with acellular dermal matrix-assisted breast reconstruction. Ann Plast Surg. 2012; 68(4):346–356. [PubMed: 22421476]

Hoganson DM, O'Doherty EM, Owens GE, Harilal DO, Goldman SM, Bowley CM, Neville CM, Kronengold RT, Vacanti JP. The retention of extracellular matrix proteins and angiogenic and mitogenic cytokines in a decellularized porcine dermis. Biomaterials. 2010; 31(26):6730–6737. [PubMed: 20576289]

Howlader N, NA.Krapcho, M.Garshell, J.Miller, D.Altekruse, SF.Kosary, CL.Yu, M.Ruhl, J.Tatalovich, Z.Mariotto, A.Lewis, DR.Chen, HS.Feuer, EJ., Cronin, KA., editors. SEER Cancer Statistics Review, 1975-2011. National Cancer Institute; Bethesda, MD: 2014.

Janis JE, O'Neill AC, Ahmad J, Zhong T, Hofer SO. Acellular dermal matrices in abdominal wall reconstruction: a systematic review of the current evidence. Plast Reconstr Surg. 2012; 130(5 Suppl 2):183S–193S. [PubMed: 23096969]

Jordan SW, Khavanin N, Fine NA, Kim JY. An algorithmic approach for selective acellular dermal matrix use in immediate two-stage breast reconstruction: indications and outcomes. Plast Reconstr Surg. 2014; 134(2):178–188. [PubMed: 25068318]

Lohsiriwat V, Petit J. Nipple Sparing Mastectomy: from prophylactic to therapeutic standard. Gland Surg. 2012; 1(2):75–79. [PubMed: 25083428]

Moore MA, Samsell B, Wallis G, Triplett S, Chen S, Jones AL, Qin X. Decellularization of human dermis using non-denaturing anionic detergent and endonuclease: a review. Cell Tissue Bank. 2015; 16(2):249–259. [PubMed: 25163609]

Nano MT, Gill PG, Kollias J, Bochner MA, Malycha P, Winefield HR. Psychological impact and cosmetic outcome of surgical breast cancer strategies. ANZ J Surg. 2005; 75(11):940–947. [PubMed: 16336382]

Petersen TH, Calle EA, Colehour MB, Niklason LE. Matrix composition and mechanics of decellularized lung scaffolds. Cells Tissues Organs. 2012; 195(3):222–231. [PubMed: 21502745]

Reimer J, Syedain Z, Haynie B, Lahti M, Berry J, Tranquillo R. Implantation of a Tissue-Engineered Tubular Heart Valve in Growing Lambs. Ann Biomed Eng. 2016

Scarritt ME, Bonvillain RW, Burkett BJ, Wang G, Glotser EY, Zhang Q, Sammarco MC, Betancourt AM, Sullivan DE, Bunnell BA. Hypertensive rat lungs retain hallmarks of vascular disease upon decellularization but support the growth of mesenchymal stem cells. Tissue Eng Part A. 2014; 20(9-10):1426–1443. [PubMed: 24378017]

Scarritt ME, Pashos NC, Bunnell BA. A review of cellularization strategies for tissue engineering of whole organs. Front Bioeng Biotechnol. 2015; 3:43. [PubMed: 25870857]

Seaman BJ, Akbari SR, Davison SP. A novel technique for nipple-areola complex reconstruction: the acellular dermal matrix onlay graft. Plast Reconstr Surg. 2012; 129(3):580e–581e.

Siegel R, DeSantis C, Virgo K, Stein K, Mariotto A, Smith T, Cooper D, Gansler T, Lerro C, Fedewa S, Lin C, Leach C, Cannady RS, Cho H, Scoppa S, Hachey M, Kirch R, Jemal A, Ward E. Cancer treatment and survivorship statistics, 2012. CA Cancer J Clin. 2012; 62(4):220–241. [PubMed: 22700443]

Wainwright D, Madden M, Luterman A, Hunt J, Monafo W, Heimbach D, Kagan R, Sittig K, Dimick A, Herndon D. Clinical evaluation of an acellular allograft dermal matrix in full-thickness burns. J Burn Care Rehabil. 1996; 17(2):124–136. [PubMed: 8675502]

Walter RJ, Matsuda T, Reyes HM, Walter JM, Hanumadass M. Characterization of acellular dermal matrices (ADMs) prepared by two different methods. Burns. 1998; 24(2):104–113. [PubMed: 9625233]

Abbreviation

TNPRC	Tulane National Primate Research Center
H&E	Hematoxylin and eosin
GAG	Glycosaminoglycans
IHC	Immunohistochemical
ECM	Extracellular matrix
BMSC	Mesenchymal stem cells
PCNA	Proliferating cellular nuclear antigen
NAC	Nipple-areolar complex
IACUC	Institutional Animal Care and Use Committee
gDNA	Genomic DNA
TUNEL	TdT-mediated dUTP Nick-end Labeling

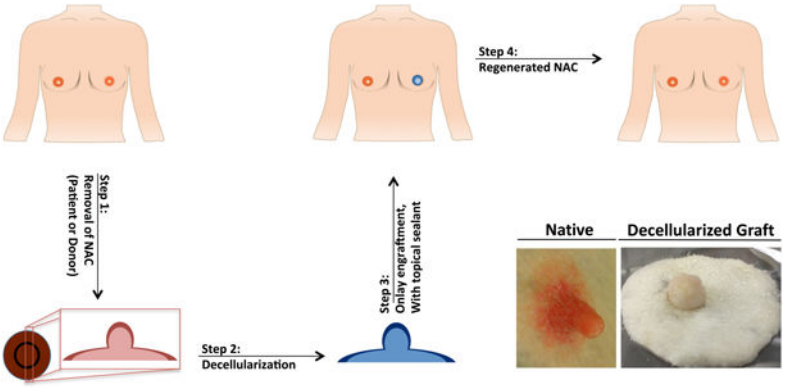

Figure 1. Schematic of the decellularization and engraftment process of the NAC

Step 1) Depicts the collection of the NAC from either the patient, who will then receive their own regenerated NAC, or a donor Step 2) decellularization of NAC graft with detergents, salts and enzyme; Step 3) onlay engraftment the acellular NAC; Step 4) allow for the patients own cells to migrate into the acellular NAC graft. Bottom Right) Representative images of native and decellularized rhesus NAC.

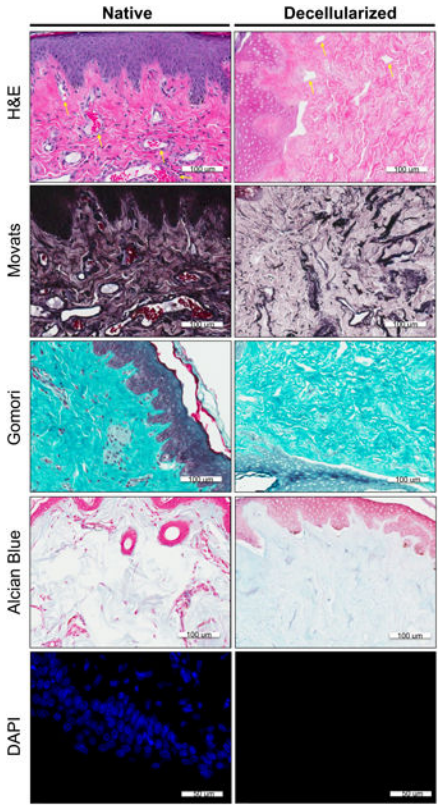

Figure 2. Histological stain and DAPI label of native vs. decellularized NAC

Each row represents a different nuclei or extracellular matrix component stain. The first column depicts the native tissue structures and the last column depicts the decellularized matrix. Row 1) H&E staining; extracellular matrix- pink, nuclear material and acidic structures-purple Row 2) Movat's staining: Nuclei and elastic fibers – black; Collagen and reticular fibers – yellow; Ground substance, mucin – blue; Fibrinoid, fibrin intense and Muscle – red. Row 3) Gomori staining: Collagen- green; nuclear and acidic structure-blue. Row 4) Alcian Blue staining: Glycosaminoglycans- light blue; nuclear material and acid structures-red. Row 5) DAPI labeling: nuclear material- bright blue

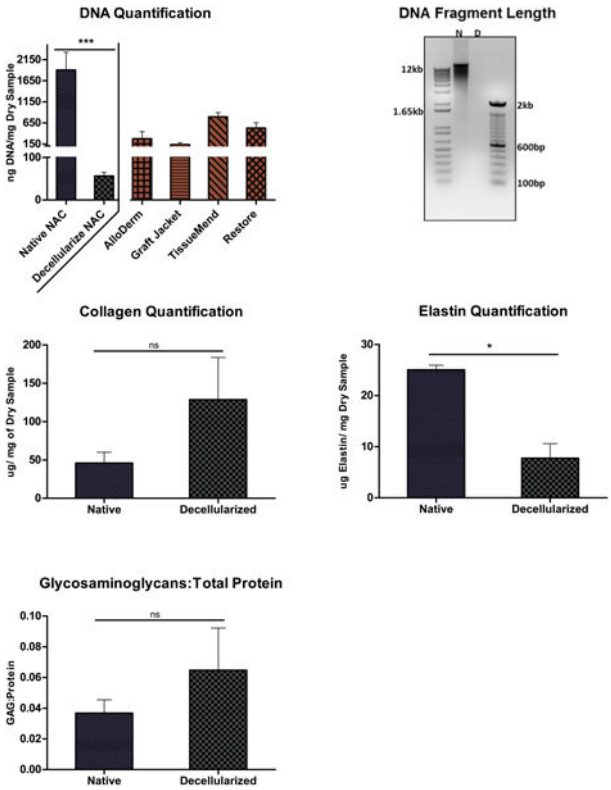

Figure 3. Quantification DNA levels and fragmentation and GAG: Protein ratio

, Top, left) Average ng DNA/mg of lyophilized tissue of native vs. decellularized matrix, values of 1905±422.1 ng and 56.51±8.45 ng, respectively; with a significant difference of $P<0.05$. Commercially available acellular product: TissueMend™, Restore™, GraftJacket™ and AlloDerm™, which have reported DNA contents of 794.6 ± 97.8, 526.8 ± 125.6, 134.6 ± 44.0 and 273 ± 169 ng DNA/mg dry tissue weight, respectively. (Choe and Bell 2001, Derwin, Baker et al. 2006, Moore, Samsell et al. 2015) Top, right) Agarose gel of native and decellularized nipple scaffold. Middle, left) Average collagen; 46.12±13.88 and 128.57±55.05 μg collagen/ dry mg samples for native and decellularized, respectively. Middle, right) Elastin quantification of decellularized and Native NAC, 7.77±2.84 and 25.03±0.93, respectively. Bottom, left) Glycosaminoglycans to Protein Concentration, with no significant different between native, 0.068±0.027, and decellularized, 0.025±0.004.

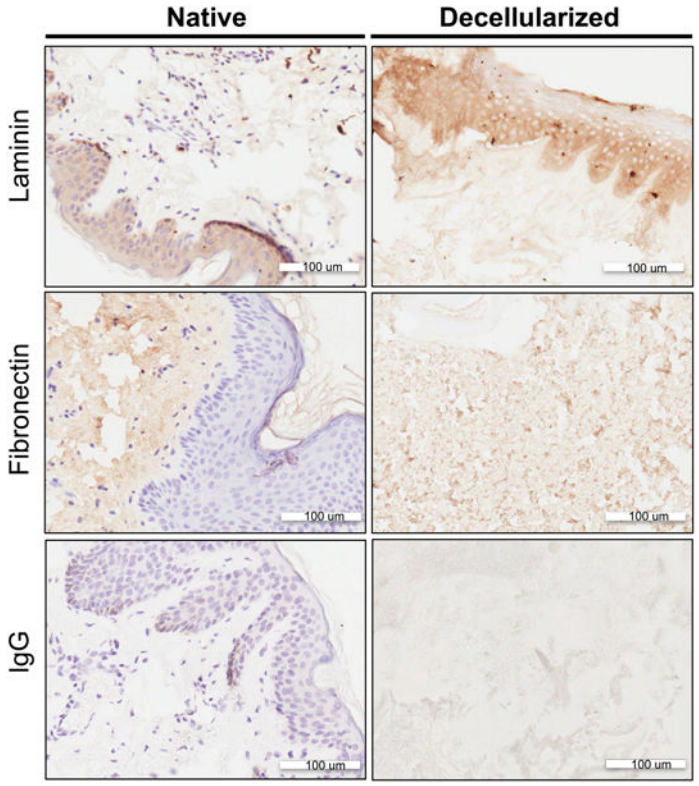

Figure 4. Immunohistologic labeling of cell adhesion molecules of native vs. decellularized NAC

, Each row represents a different nuclei or extracellular matrix component stain; Row 1) Fibronectin, Row 2) Laminin, Row 3) IgG controls. The first column depicts the native tissue structures and the second column depicts the decellularized matrix. The secondary antibody with a HRP attached was developed with DAB, which developed the antigen of interest a brown color. The counterstain of the nuclei is shown as purple staining.

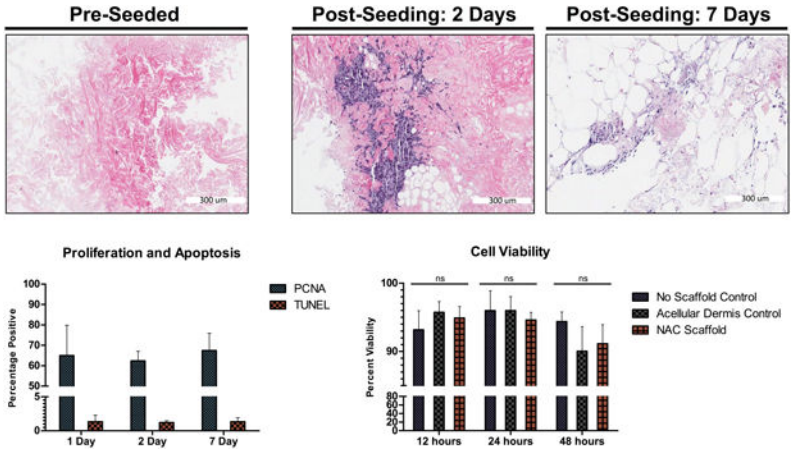

Figure 5. Cell proliferation and apoptosis, and cell viability

, Top row shows the acellular NAC scaffold before were added to culture, and cells beginning to migrate into areas of the NAC scaffold at 2 days and 7 days. Bottom, Left PCNA and TUNEL Day 1, 2 and 7 days post-seeding of cells on the acellular NAC, 64.98±7.42%, 62.38±2.34%, 67.42±4.23% and 1.34±0.48%, 1.21±0.14%, 1.34±0.3%; respectively. Bottom Right, Cell Viability at 12 hours, 24 hours, and 48 hours; no scaffold control: 93.18±1.39% (12hrs), 95.98±1.45% (24hrs), 94.39±0.69% (48hrs); commercially available acellular dermis control: 95.18±0.79% (12hrs), 95.97±1.03% (24hrs), 90.39±1.18% (48hrs); decellularized NAC scaffold: 94.92±0.95% (12hrs), 94.59±0.65% (24hrs), 91.14±1.62% (48hrs).